ACOUSTIC EMISSION WELD MONITORING IN THE 2195 ALUMINUM-LITHIUM ALLOY

Due to its low density, the 2195 aluminum-lithium alloy was developed as a replacement for alloy 2219 in the Space Shuttle External Tank (ET). The external tank is the single largest component of the space shuttle system. It is 154 feet long and 27.6 feet in diameter, and serves as the structural backbone for the shuttle during launch, absorbing most of the 7 million plus pounds of thrust produced. The almost 4% decrease in density between the two materials provides an extra 7500 pounds of payload capacity necessary to put the International Space Station components into orbit. The ET is an all-welded structure; hence, the requirement is for up to five re-welds without hot cracking. Unfortunately, hot cracking during re-welding or repair operations was occurring and had to be dealt with before the new super lightweight tank could be used. Weld metal porosity formation was also of concern because it leads to hot cracking during weld repairs. Accordingly, acoustic emission (AE) nondestructive testing was employed to monitor the formation of porosity and hot cracks in order to select the best filler metal and optimize the weld schedule.

The purpose of this work is to determine the feasibility of detecting hot cracking in welded aluminum-lithium (Al-Li) structures through the analysis of acoustic emission data. By acoustically characterizing the effects of reheating during a repair operation, the potential for hidden flaws coalescing and becoming "unstable" as the panel is repaired could be reduced. The term "unstable" refers to the tendency of microcracks present from a previous weld pass to join together, forming a critically sized defect upon re-weld. Identification of regions where microcrack growth is likely to occur and the location of active flaw growth in the repair weld, as it is performed, will provide the welder with direct feedback as to the current weld quality enabling adjustments to the repair process be made in the field. An acoustic emission analysis of the source mechanisms present during welding has been conducted with the goals of locating regions in the weld line that are susceptible to damage from a repair operation, identifying the formation of critically sized flaws and providing accept/reject criteria for the quality of a weld as it is performed.

The acoustic signals generated by a material under load provide a means to both qualitatively and quantitatively monitor structural integrity. Each source mechanism has a somewhat unique acoustic signature varying in duration, amplitude, energy, frequency, etc. Two approaches have classically been used to identify the type of failure within a material; full waveform (frequency) and parametric (characteristic signal features).

The parametric approach takes the output voltages from the sensors mounted to the structure and through timing and threshold values, preset by the test conductor, captures the essence of the individual acoustic signals in a set of descriptive features including peak amplitude, rise time, duration, energy and counts. On the other hand, the waveform based approach stores the entire "digitized" waveform over a predetermined time period. The power spectrum of the digitized acoustic signal is computed through a fast Fourier analysis yielding the intensities of the embedded frequency components. Both techniques have merit and deficiencies as to be described later. The analysis of the Al-Li AE data presented herein looks at each of the two standard techniques as well as takes the best features of each, generating a hybrid parametric-waveform (PaW) approach. The PaW analysis technique is based upon identifying variations in the characteristics obtained from the parametric and frequency domain signal features. The analysis of the data from each approach is conducted through the use of an unsupervised artificial neural known as a self organizing map (SOM). In order to help determine the nature of the acoustic signal clusters found with the SOM, tensile tests on small sections cut from a repair panel are conducted and compared to the repair weld results.

ACOUSTIC EMISSION TESTS AND RESULTS

A total of 137 manual TIG repair welds consisting of one or more fill and cover passes were made on ten weld specimens; two $0.207 \times 5.9 \times 24.0$ inch panels of 2195 Al-Li alloy joined together with variable polarity plasma arc (VPPA) welding. The samples were monitored acoustically with PAC (Physical Acoustics Corporation) WDI (Wide band Differential Integrated amplifier) sensors that were attached using hot melt glue.

Re-welding was performed in 4 inch segments along the length of the initial weld, separated by three inch sections of the initial weld, Figure 1. The repair process began by planishing the bead flush with the panel surface over the repair region. A high-speed router was then used to create a slot in the weld material to approximately the mid-thickness point over the center of each repair zone and faired to the surface of the plate. Tungsten inert gas (TIG) repair welds that consisted of one or more fill passes were

finally made on the ten specimens as the AE signals were collected and examined.

Two PAC WDI sensors were used along with the PAC DSP (Digital Signal Processing) card to record the repair weld acoustic activity. During all weld repairs the AE system timing, threshold and location parameters were set to the values provided in Table 1. The AE sensors were arranged to provide linear location capabilities along the length of each repair zone while allowing adequate room for the welder to work and enough separation from the weld zone to prevent heat damage to the sensors. The three sensor location sets are defined as "P-A", "P-B" and "P-C" in Figure 1. The sensors were bonded with hot melt glue seven inches apart and three inches off the weld centerline as previously mentioned. The hot melt glue provided an added degree of protection from the weld heat by softening and releasing before the sensors could be damaged. Lead breaks, 0.5 mm 2H, were performed after resetting the sensors for each repair zone to ensure that good and consistent sensor coupling was maintained for each repair cycle. A good sensor bond was defined as one where lead breaks, one inch from the sensor, produced a peak amplitude of 70 to 80 dB.

AE Parameters	Peak definition time (PDT)	1000 µs
	Hit definition time (HDT)	2000 µs
	Hit lockout time (HLT)	2000 µs
	Sensor gain	40 dB
	Threshold	45 dB
Location Parameters	Wave speed	185000 inch/sec
	Lockout	7 inch
	Overcalibration	0.5 inch

Table 1. AE system initialization file repair welds.

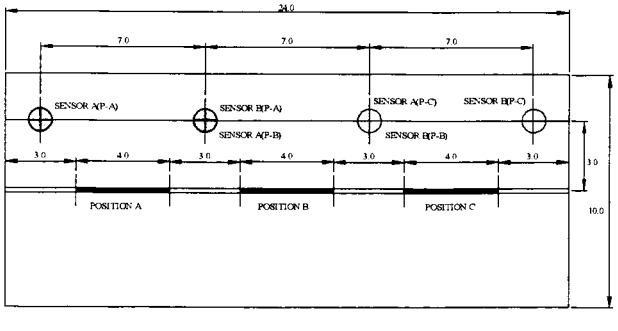

Figure 1. Sensor placement for weld repairs.

In addition to the re-weld samples, diamond saw notched tensile samples were low cycle fatigue loaded to generate "clean" crack signals, free from background weld noises, to use in comparison against the re-weld network model results. Here, the acoustic activity from five tensile coupons, cut from an Al-Li repair panel, were monitored with a single WDI sensor connected to a PAC DSP card during the low cycle fatigue loading. The sensor was centered just above the weld line and again bonded to the sample with hot melt glue.

The tensile specimens were manufactured from a weld repair panel by cutting 1.0 inch wide strips perpendicular to the weld. A 0.08 inch deep notch was cut through the thickness of the specimen in the center of the weld with a diamond wheel saw to provide a crack initiation point. The samples were gripped in a 20 KIP tensile test machine and cycled to failure. The tensile tester was configured to provide a positive (tensile) 0.2 Hz sinusoidal loading. The system settings for the PAC DSP MISTRAS program were the same as those used for the weld repair monitoring except that a larger 50 dB threshold was required to overcome the hydraulic cavitation noises of the tensile tester.

The parametric, waveform energy and PaW data were tabulated from all five specimens into ASCII files suitable for testing the trained neural networks. Here, to provide some commonality between the test results for each method, only those crack signals which could be identifiable in the parametric and waveform records were included in the test files. The individual signals were identified and matched based upon the time stamp given to each signal.

During the course of this research effort four acoustic signals were found to be produced most frequently. An example of these signals and there resulting power spectrum plots are shown in Figures 2 through 5. The first signal type (Figure 2) has been found to occur when critically sized cracking (visible by x-ray or by physical observation) is present in the weld. The signal is characterized as having a peak amplitude greater than 65 dB (1.8 volt after 60 dB gain) with a relatively large rise time, number of counts and energy value. The waveform (frequency) characteristics show three peak intensity regions located around 100, 300 and 600 kHz.

Signal type two, Figure 3, was found to occur most frequently in welds which showed a large amount of porosity and those that had seen multiple repair passes. The signal was similar in shape to a type 1 signal except that its amplitude and energy

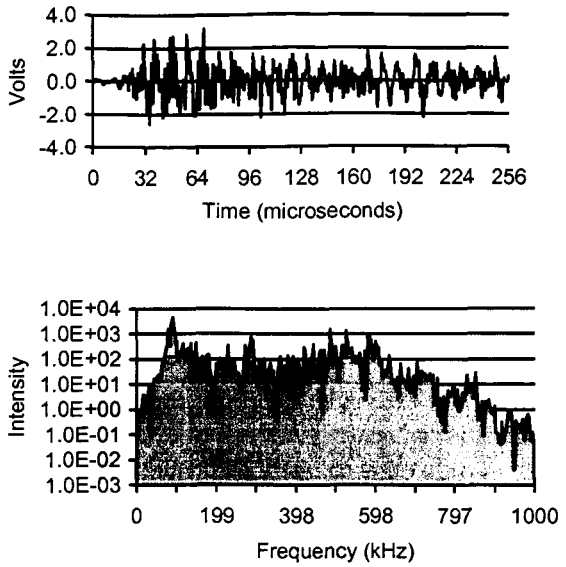

Figure 2. Signal Type 1: Hot Cracking.

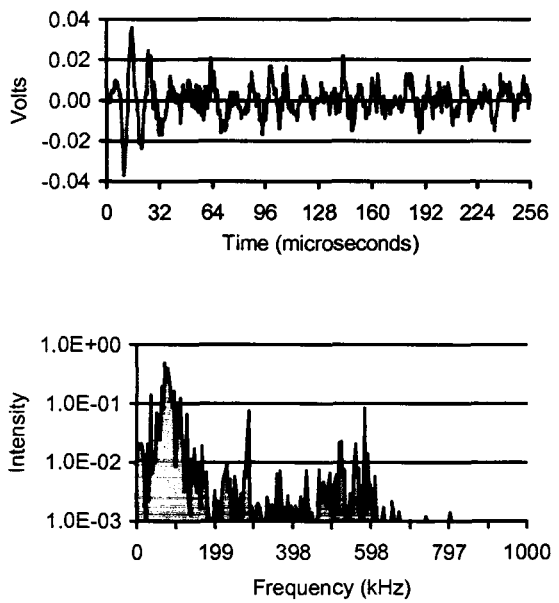

Figure 3. Signal type 2: Microcracking.

parameters were much weaker. This was also apparent in the power spectrum, in that the same three peaks were present but with much less intensity.

The strength and number of these signals were found to increase with the number of repair passes up to a point where major crack initiation began forming the type one signal. In other words, a large number of type two signals during a repair pass indicates that the region is susceptible to hot cracking damage from future repair passes.

A lithium hydroxide scale was observed to form on the surface of the repair weld as a result of the high temperatures involved in the first pass of both the VPPA and TIG welds. The porosity that occurred during the second or cover pass of the TIG welded repair was the result of the incomplete removal of this hydroxide scale prior to making the cover pass. From the data collected, both porosity and hot cracking were seen to be minimal during the initial weld, but began to occur more frequently with the increase in subsequent passes, indicating that the effect is cumulative: with more re welds, there is an increased chance and extent of hot cracking.

Low frequency (100 kHz) signals, Figure 3, were generated as a result of the weld puddle being formed and flowing during the weld operation. The amplitudes and energies of these signals were generally small with rise times that were similar to the type one signal. In certain instances very large, up to 90 dB, low frequency signals were produced and were thought to be caused by the welder bumping the panel with the welding rod.

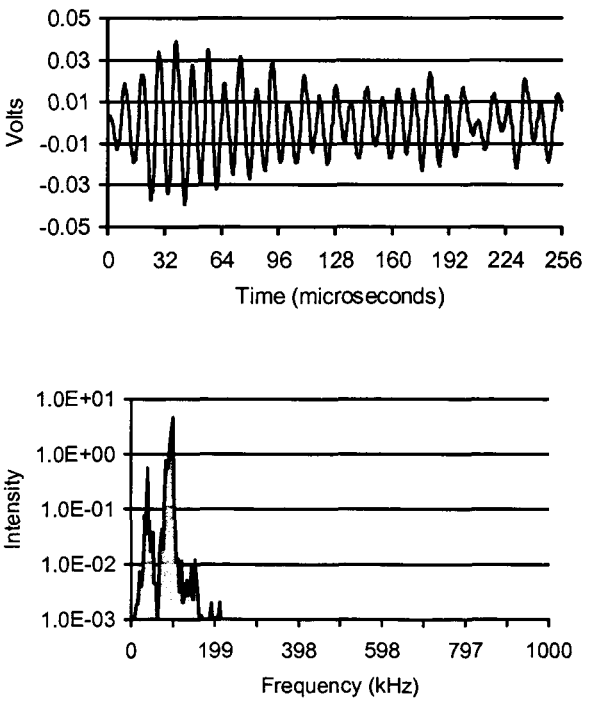

Figure 4. Signal type 3: Rubbing/weld flow.

In certain instances, during the repair, abnormal weld arcing produced spikes in the recorded waveforms. These signals had large amplitudes and energies with

small rise times and number of counts, Figure 5. The power spectrum of these signals would essentially be a flat line out past 1 MHz due to the Dirac delta function nature of the spike.

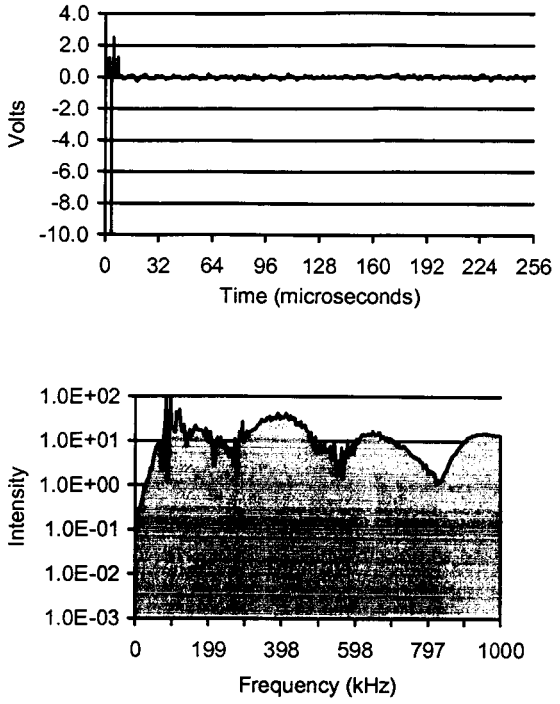

Figure 5. Signal type 4: Spark noise.

If the acoustic signals were as well behaved as these examples and as few in number, identification of hot cracking would be no problem. However, the signals presented are ideal in nature, when in reality, due to source arrival time overlap, flaw location, number of signals, etc. it is very difficult to sort each signal by hand. The problem therefore is to develop a neural network mode to classify each signal by first categorizing all of the signals recorded during the weld into a particular signal class and secondly to identify the mechanism that creates each signal.

NEURAL NETWORK DATA ANALYSIS

Self organizing map artificial neural networks (ANN) were developed using NeuralWorks Professional II/plus software by NeuralWare to map features of the parametric, waveform and PaW data. The SOM is a two layered network (Figure 6), utilizing an input and a Kohonen layer. In the input layer, data is ordered and presented to the network as an N-dimensional input vector. As an example, "N" could represent the signal rise time, counts, energy and amplitude from the parametric AE data set. The Kohonen layer, which is fully connected to the input layer, provides a two dimensional grid of neurons, through which unsupervised learning takes place. The result of training the SOM network is a topological map of the multidimensional input vector space, where order is preserved through a grouping of input data with similar features: The SOM performs the data clustering through a minimization of the Euclidean distance between the Kohonen layer weights and each input data vector.

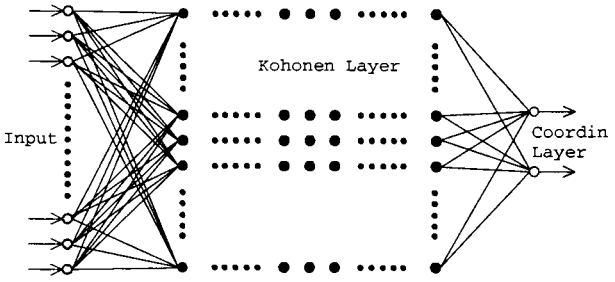

Figure 6. Architecture of a SOM neural network.

The training process consists of introducing the network to as many of the test related variables as possible and then to identify the clusters from within the output grid to known acoustic mechanisms. A useful feature of the software for data clustering is that the network can interpolate between the individual neurons during the test phase, producing X-Y coordinates for each input test vector. In doing so a continuous map of the N-dimensional input vectors is produced over the 2-dimensional grid extending in value from -1.0 to +1.0 along both axis

Three SOM neural networks were trained, using the parametric, waveform energy and PaW AE data, for 20,000 cycles each on the weld data using networks featuring a 10 by 10 Kohonen layer.

PARAMETRIC

The first network was presented four dimensional input vectors (rise time, counts, energy and amplitude) for each of the 671 signals stored in the data from several weld cycles. Here, the details of the parametric and waveform signals could be compared to gain a better estimate as to each source mechanism. By searching the associated waveform files, an estimate as to the source of the acoustic event could be made based upon notes taken during the weld repair and the frequency/intensity data from the waveforms. Overall, only nine type one and nine type four signals were found in the cumulative AE data. The remaining signals were divided between the type two and three signals.

An X-Y map was generated by the SOM of the clustered input vectors. At this stage in the analysis identification of individual clusters from within this result file is difficult, if not impossible, without some knowledge of the input vector values. In order to better understand the results of the SOM the average amplitudes, energies, rise times and counts were computed and are shown in Figures 7 through 10. The plots show that the network clustered the highest amplitude, energy, rise time and count signals around the (0.0, -0.4) coordinate. These signals all had amplitudes ranging from the mid sixties up to 97 dB, average energies in excess of 200 and over 1000 counts. The rise times though varies from as small as 1 μs to nearly 5000 μs.

Due to the magnitude of these signal parameters, it was hypothesized that this cluster may represent weld crack activity. To investigate this hypothesis and determine the decision boundaries for the cluster, the parametric data was screened against the waveform time and frequency data in an attempt to identify the various signal types. Figure 11 shows graphically the results of this exercise. Notice that the nine "type one" signals all cluster in the region bordered by $-0.20 < X < 0.60$ and $-0.20 < Y < -0.60$. Within this region three of the nine, type 4 signals are also captured along with one type 2 signal. None of the low amplitude-low frequency, type 3 signals, were included in the cluster.

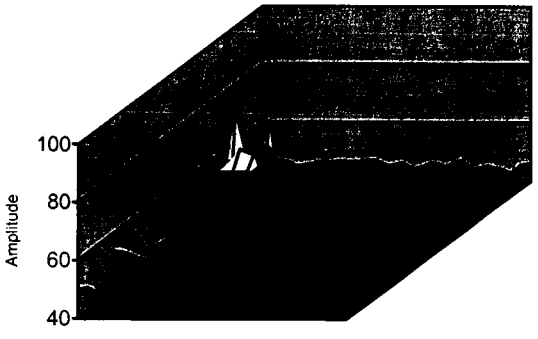

Figure 7. Average amplitudes from parametric SOM.

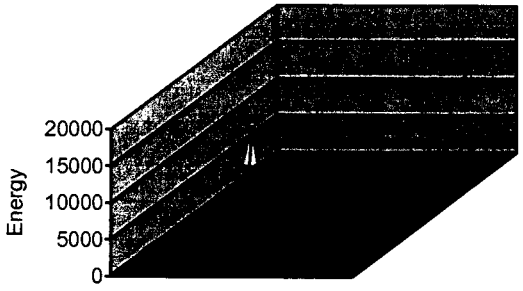

Figure 8. Average energies from parametric SOM.

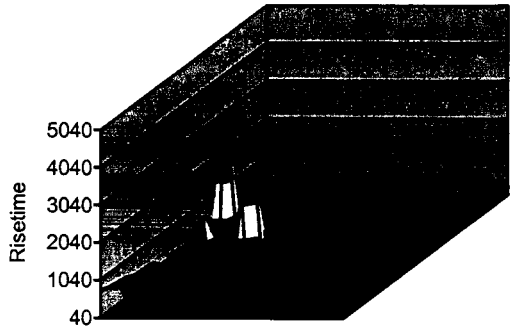

Figure 9. Average risetimes from parametric SOM.

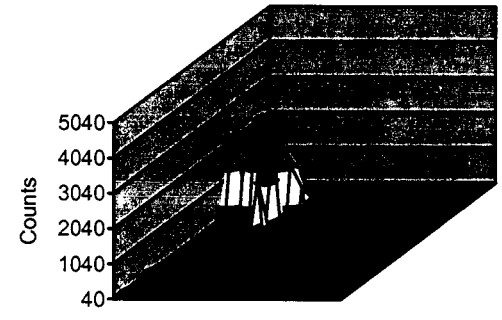

Figure 10. Average counts from parametric SOM.

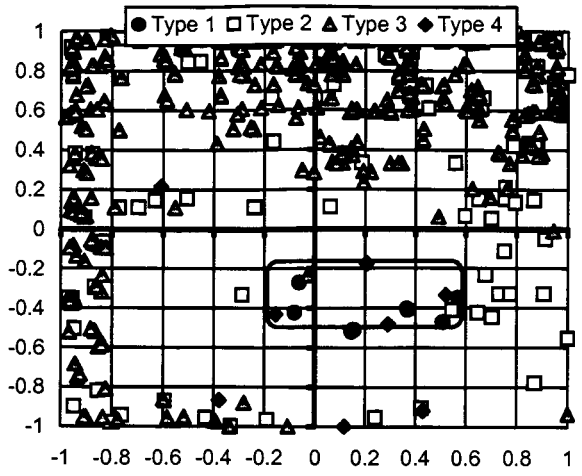

Figure 11. Signal type map for parametric data.

WAVEFORM ENERGY

The second network was presented with the same 671 training AE signals as used for the parametric study. Four dimensional vectors made-up of the partitioned waveform energy served as inputs to the network. The vectors were computed by summing the area under the power spectrum over four 250 kHz bands up to 1.0 MHz.

The average values for the energy clusters were again computed for the SOM. A main peak is found to occur in the region $-0.7 < X < -0.6$ and $-0.2 < Y < -0.1$ for all the energy intervals. Secondary peaks how up in all but the lowest (0 to 250 kHz) energy band indicating that variations do exist in the higher frequency components of the signals that may correspond to individual signal types.

Using the same criterion as for the parametric data, a boundary could be placed around the type 1 signals, as shown in Figure 12. Overall, the network does not cluster the waveform energy data as well as it had with the parametric data. The separation between the type one and other source mechanisms is not as defined or complete. The network may be keying on the overall magnitude of the signal energies and not to the relative scale of energies from each signal. Both low and high frequency signals with common total energy values may look the same to the network.

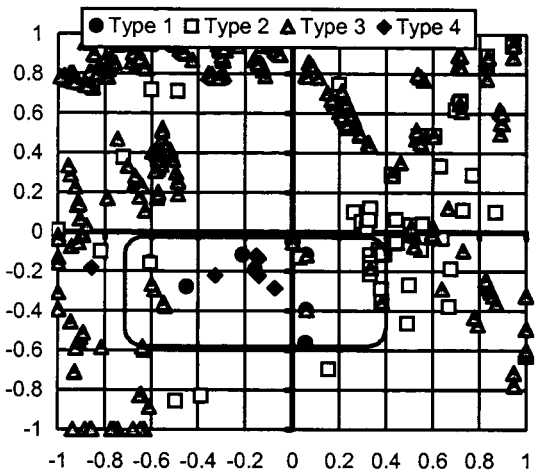

Figure 12. Signal type map for waveform energy data.

COMBINED PARAMETRIC AND WAVEFORM ENERGY

Combining the parametric and waveform energy data into a single training file produced the tightest and cleanest cluster of type one signals. As shown in Figure 13, the network clustered the "crack" signals between $0.0 < X < 0.8$ and $0.3 < Y < -0.1$. Within this cluster only five type four signals were found and none of the type two or three signals were present.

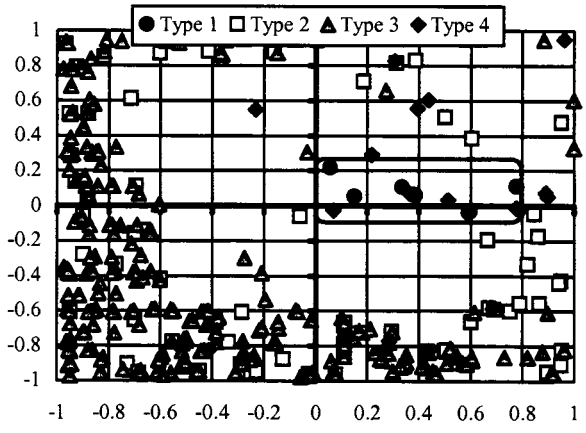

Figure 13. Signal type map for PaW data.

TENSILE TEST

The cumulative AE data collected from the tensile tests was edited to contain only the crack signals that were common to all three analysis formats. Thirty-four signals in all were found that could be traced to known crack growth activity.

When the parametric data was presented to the trained network (Figure 14) only three signals fell within the type 1 cluster. With the exception of five signals the tensile data instead, clustered in a region away from the type one zone. At first this would seem to indicate that the type one zone was in error, but the real reason is most likely an attenuation effect. The weld data was taken with the sensors located up to 12 inches from the source while the tensile tests were conducted with the sensor only 1 to 2 inches from the crack initiation point. Also, the acoustical variations between crack initiation due to welding and during tensile testing may be more different than previously expected. The same trend was found when the PaW tensile data was tested on the previously trained SOM (Figure 16).

Surprisingly the waveform energy tensile AE data clustered the closest to the type one zone as shown in Figure 15. Most of the signals fell within the zone, while the remainder bordered the zone. Apparently the frequency content of the crack initiation signals is similar enough between tensile testing and weld repair hot cracking that the network could identify the source.

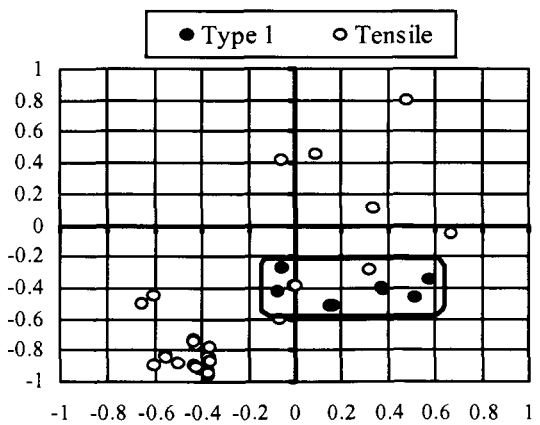

Figure 14. Parametric tensile data clusters.

CONCLUSIONS

The process through which acoustic emission signal analysis can be used to detect the onset of hot cracking during weld repairs of aluminum-lithium has been demonstrated. A self organizing neural network has shown the ability to separate the AE data into clusters based on the relative magnitudes of their descriptive features. A waveform, parametric and combined approach were all used to characterize the formation of hot cracking during weld repair.

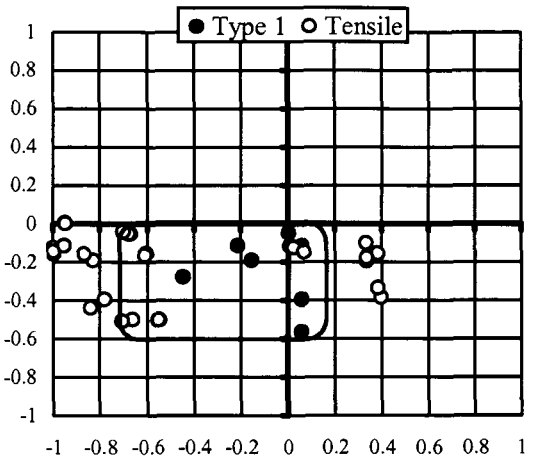

Figure 15. Waveform energy tensile data clusters.

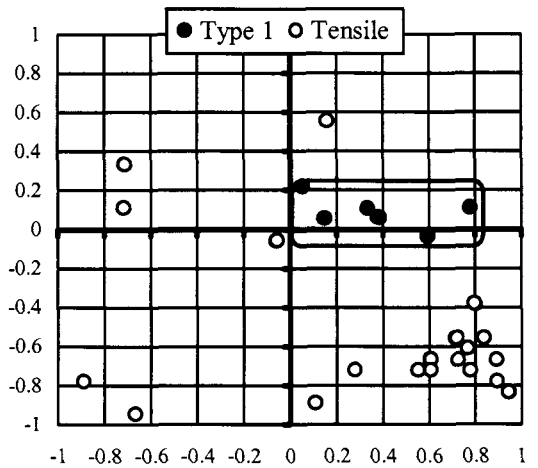

Figure 16. PaW tensile data clusters.

Overall, the hot cracking signals were characterized as having peak frequencies at 100, 300 and 600 kHz along with moderate to high amplitudes and energies. The amount and magnitude of the acoustic activity would increase from reweld to reweld until final coalescence of the microcracks and/or porosity lead to final formation of large scale cracking. In some cases these cracks would be visible, but normally only X-Ray would show the extent of damage.

The results were verified through low cycle fatigue testing on small tensile samples cut from a repair welded panel. A limited number of "clean" crack signals were produced from these tests and mapped against the signal clusters determined by the neural network. The largest of these crack signals fell within the boundaries of the hot cracking clusters.